

Cathodoluminescence and electron beam induced current study of partially relaxed AlGaAs/GaAs/InGaAs heterojunction phototransistors under operating conditions

O. Sjölund^{a)}

Department of Optoelectronics and Electrical Measurements, Chalmers University of Technology, 412 96 Göteborg, Sweden

H. T. Lin and D. H. Rich

Photonics Materials and Devices Laboratory, Department of Material Science and Engineering, University of Southern California, Los Angeles, California 90089-0241

M. Ghisoni and A. Larsson

Department of Optoelectronics and Electrical Measurements, Chalmers University of Technology, 412 96 Göteborg, Sweden

S. Wang

Department of Microwave Technology, Chalmers University of Technology, 412 96 Göteborg, Sweden

J. Thordsson and T. G. Andersson

Department of Physics, Chalmers University of Technology, 412 96 Göteborg, Sweden

(Received 27 December 1996; accepted for publication 28 April 1997)

We have studied time-resolved cathodoluminescence (CL) and electron beam induced current (EBIC) on AlGaAs/GaAs/InGaAs heterojunction phototransistors under operating conditions, i.e., at room temperature and under bias. Devices from four wafers, with a different amount of lattice relaxation, were tested. It is shown that the CL intensity increases more than one order of magnitude as the voltage is increased and the current gain of the device turns on. The voltage dependence of the CL signal is analogous to the current–voltage curve of the transistor. The buildup in CL intensity was found to be much less in devices with low current gain showing that the CL intensity correlates to the electrical gain of the device. Time resolved CL showed two distinct CL decay times, one very short, a few nanoseconds, and one long, of the order of microseconds. This indicates that two fundamental recombination processes are present, which we attribute to a spatially direct recombination between carriers in the base and a spatially indirect recombination. This spatially indirect recombination is believed to come from recombination of electrons trapped in the notch formed at the conduction band discontinuity and holes in the base. By studying EBIC as a function of beam current for devices from the different wafers we found that relaxed devices have a complex current-gain relationship. They require higher current densities than nonrelaxed devices to reach high gain. At low current densities the gain is very low and the ideality factor is high indicating a high degree of trap related recombination. At high current densities, on the other hand, these traps become filled and the associated recombination quenched. This results in a gain and an ideality factor comparable to those of nonrelaxed devices. © 1997 American Institute of Physics. [S0021-8979(97)04315-6]

I. INTRODUCTION

Cathodoluminescence (CL) and photoluminescence (PL) have become widely used tools for characterization of the optical properties of III–V semiconductor materials,^{1–12} in particular because these measurements are nondestructive and can be performed on whole wafers.⁴ These techniques have even been used for material characterization on an atomic scale.^{13,14} Several studies have used low-temperature CL^{6,10,11} and PL^{4,5,7–9} to predict device parameters. Yuan *et al.*¹ found an unexpected PL peak originating from the AlGaAs/GaAs heterojunction. It was shown that this peak, known as the *H* band, came from a spatially indirect transi-

tion of carriers trapped in the notch formed by the conduction band discontinuity with carriers in the valence band close to the valence band discontinuity. A schematic band diagram illustrating this recombination is included in Fig. 1. Since the recombination is spatially indirect the carrier lifetime is expected to be long. If the heterojunction is a *p-n* junction then the PL intensity of this peak has a strongly nonlinear dependence on the optical excitation intensity.⁷ The wavelength and width of the peak are also dependent on the excitation intensity. This *H* band has been studied widely^{1,2,5} and it has been shown that it can be used to predict the performance of devices using heterojunctions, such as heterojunction bipolar transistors (HBTs), prior to device fabrication.^{4–9} Several authors have found correlations between the CL or PL signal and the device properties such as the electrical gain, β , of HBTs.^{4,6,8} However, most of these studies have been at low temperatures (1.4–77 K), far below

^{a)}Work done at: Photonics Materials and Devices Laboratory, Department of Material Science and Engineering, University of Southern California, Los Angeles, CA 90089-0241; Electronic mail: ola@elm.chalmers.se

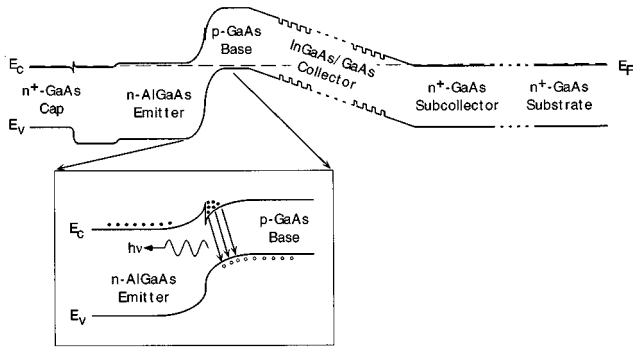


FIG. 1. Schematic band diagram of the nominal structure. The inset shows an enlargement of the notch region under bias. The proposed spatially indirect recombination is shown (see Refs. 1, 2, and 5). Electrons are trapped in the notch formed at the conduction band discontinuity due to the slight field caused by the collector-emitter voltage. Holes are accumulated in the base at the valence band discontinuity. Since the recombination is spatially indirect the lifetime is expected to be long.

the operating temperature of these devices, and at zero bias. At these temperatures built-in fields in the device might be affected by carrier freezeout. Very few PL or CL studies have been made on actual devices under operating conditions, i.e., at room temperature and bias.^{10,11}

Our particular interest lies in heterojunction phototransistors (HPTs).¹⁵ HPTs are, due to their inherent gain and ability to be vertically integrated with other components, attractive for future optical interconnection and processing systems.^{16–18} HPTs in the AlGaAs/GaAs/InGaAs material system are of particular interest since GaAs-based technology is mature, particularly vertical cavity surface emitting lasers (VCSELs).¹⁹ Vertical integration of these HPTs with, e.g., reflection modulators²⁰ or VCSELs²¹ has been shown. If combined with VCSELs, it would be desirable to use such VCSELs in a bottom emitting configuration. This allows the further integration of beam controlling optical elements on the substrate side.²² To achieve this, the laser emission wavelength needs to be beyond the absorption region of the substrate, i.e., for GaAs (the substrate used in this work) longer than ≈ 900 nm. High performance VCSELs operating well beyond 900 nm exist, based upon compressively strained InGaAs quantum wells (QWs),²³ hence the desire to produce HPTs which also operate at these wavelengths.

HPTs normally consist of a wide band-gap *n*-AlGaAs emitter, a *p*-GaAs base, and an *n*-GaAs collector. The optical absorption is achieved by inserting absorptive material into the collector region. The photogenerated electrons drift towards the substrate and photogenerated holes drift towards the base, giving rise to a base current. Increasing the thickness of absorbing material will produce an increase in overall device efficiency, greater than the increase in absorption because the gain is a nonlinear function of the collector current.²⁴ Unfortunately, the absorptive material required, as for the VCSELs, is InGaAs, which is lattice mismatched relative to the GaAs substrate. This introduces a tradeoff in the design as one cannot simply increase the InGaAs thickness, since when the critical thickness is exceeded the lattice will no longer be able to accommodate the strain and will

relax,²⁵ giving rise to defects which one would expect to degrade the electrical characteristics of the devices. To overcome the above, two different design strategies are open to us: placing the absorber in a resonant cavity to enhance the absorption^{26,27} or increasing the amount of absorptive material and accepting some degree of lattice relaxation. Interestingly, lattice relaxation may not necessarily be catastrophic and may be tolerated to some degree if an enhancement in overall performance is still achieved. Work showing that partially relaxed multiple QW (MQW) structures can still function as photodetectors²⁸ and modulators²⁹ has been reported. Ramberg *et al.*³⁰ reported the use of partially relaxed InGaAs as the base within a HBT without any apparent performance loss. We have also previously shown that a high performance HPT operating at beyond 950 nm can be fabricated from partially relaxed material.³¹

In this paper we employ electron beam induced current (EBIC) and time-resolved CL to study HPTs under operating conditions, at room temperature and under bias, and show that there is a correlation between the electrical gain of the device and its CL signal. Time resolved CL shows that the dramatic increase in CL intensity seen when the transistor turns on has a very long decay time. Using EBIC and photocurrent measurements we have determined both the large and small signal ideality factors for the HPTs. Finally, we show a comparison between devices with different relaxation which confirms that a small amount of relaxation is indeed tolerable without catastrophic breakdown. The more relaxed devices require higher collector-emitter current than the non-relaxed devices to reach high gain and low ideality factor.

II. EXPERIMENT

Four different HPT structures were grown. The number of QWs in the collector, and thus the amount of lattice relaxation, is the only difference between the nominal structures. The HPTs are of an *n-p-i-n* configuration grown by solid source molecular beam epitaxy on an *n*-type GaAs substrate, with a constant growth temperature of 580 °C, except for the MQW region where 520 °C was used. Firstly a 1- μm *n*⁺-GaAs subcollector layer was grown followed by a 1- μm intrinsic collector region (doped less than $1 \times 10^{15} \text{ cm}^{-3}$). Then came a GaAs base of 1000 Å, *p* doped to $5 \times 10^{17} \text{ cm}^{-3}$, an AlGaAs emitter doped *n* type to $5 \times 10^{17} \text{ cm}^{-3}$ for the first 2000 Å and then $3 \times 10^{18} \text{ cm}^{-3}$ for the subsequent 1000 Å and finally 1000 Å of *n*⁺-GaAs to act as a contact layer. The 1- μm intrinsic collector region consisted of GaAs within which was buried the InGaAs MQW region of 6, 12, 20, and 30 QWs, respectively. The QWs in all four cases consisted of nominally 80 Å $\text{In}_{0.13}\text{Ga}_{0.87}\text{As}$ wells separated by 150 Å GaAs barriers. The MQW region was placed in the center of the intrinsic collector.^{31,32} Except for the six QW structures, all the structures showed evidence of cross hatching on the surface, i.e., lattice relaxation, with the level increasing with increasing number of QWs. A schematic band diagram of the nominal structure without bias is shown in Fig. 1. The inset is an enlargement of the emitter-base heterojunction, with the notch described above, under bias. The built-in field across the fully depleted MQW region

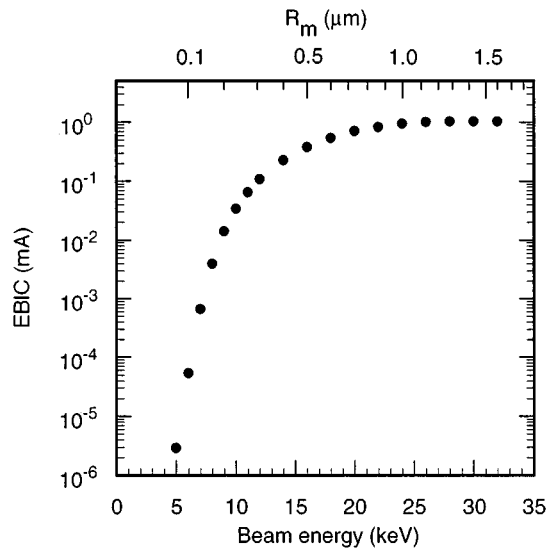


FIG. 2. EBIC as a function of beam energy, and corresponding depth, R_m , where a maximum electron-hole pair generation rate occurs, for a 6 QW device. Note that the electron range, R_e , is about 3.5 times R_m .

will produce a drift of the photogenerated carriers, with holes drifting towards the base and electrons towards the substrate.

Square devices of different sizes, ranging from 50 to 500 μm sides, were fabricated using standard photolithographic techniques and wet chemical etching. The AuGe/Ni/Au emitter and collector Ohmic contacts were deposited on the top contact layer and the substrate, respectively. For this study square devices with 200 and 500 μm sides were chosen. The devices had square optical windows with 100 and 400 μm sides, respectively.

CL, EBIC, and photocurrent measurements were performed with a modified JEOL 840-A scanning electron microscope. The details of the system have been reported previously.^{10,11} All measurements in this study have been performed at room temperature. Figure 2 shows the EBIC, at a 1 V collector-emitter voltage, as a function of beam energy, and the associated depth, R_m , where a maximum electron-hole pair generation rate occurs,³³ for an HPT with 6 QWs. The turn on of the transistor action as the beam-induced excitation reaches the base-collector depletion region is clearly shown. For the subsequent measurements, a beam energy of 22 keV has been used. At 22 keV the excitation is fairly uniform throughout the structure and R_m is about 0.9 μm , resulting in a small excitation in the subcollector. A beam current of 5 nA was used for the CL measurements (unless otherwise stated). All measurements were spatially averaged over approximately $50 \times 50 \mu\text{m}$.

Temporally resolved CL was taken with a repetition rate of 1 MHz and a duty cycle of 5%–14%. Temporally and spectrally resolved CL was measured by acquiring the CL-decay transients at different wavelengths, in increments of 1 nm. By taking the CL intensity at different time windows for each wavelength, a spectrum at each time window is obtained. For the ideality factors, the EBIC as a function of beam current was used. This gives the large signal ideality factor. For the small signal ideality factor, i.e., the gain of a

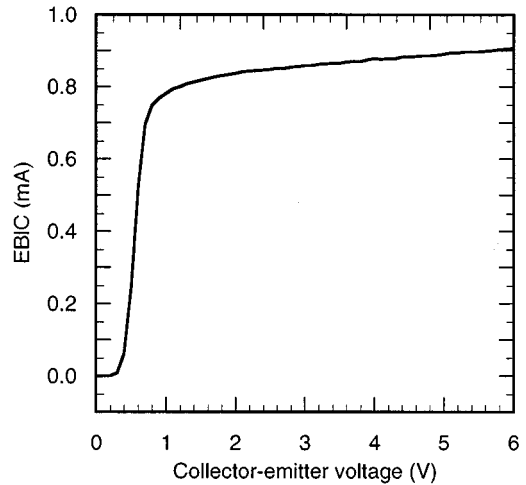


FIG. 3. EBIC as a function of collector-emitter voltage for a 6 QW device. The beam energy is 22 keV.

modulated signal as a function of a large dc current, photocurrent was used. The photocurrent was measured by using a microscope lamp as an optical source. The light was mechanically chopped and entered the system through the same monochromator used for the CL measurements. The photocurrent was then measured by a standard lock-in technique. EBIC, at different beam currents, was used to generate the dc current in the device.

III. RESULTS

EBIC as a function of collector-emitter voltage for a 6 QW device is shown in Fig. 3. This is analogous to regular I - V plots of transistors and the transistor action is clearly shown. CL spectra for the GaAs emission at different collector-emitter voltages are shown in Fig. 4(a). At 0 V two peaks are seen, one at 860 nm and the other at 875 nm. However, when the HPT turns on at about 0.5 V the short wavelength peak becomes dominant and the CL intensity increases significantly. Figure 4(b) shows that the CL intensity increases by more than an order of magnitude. We also see that the CL and EBIC signals have the same voltage dependence. Devices with poor responsivity, and thus low electrical gain, have much less, or no, increase in CL intensity with voltage showing that the CL as a function of voltage can be used as a good probe of device performance.

Time resolved measurements of the dominant 860-nm GaAs peak in Fig. 4(a) were performed, and are presented in Fig. 5. At 0 V the CL decay is very fast with a $1/e$ -decay time, τ_i , of about 1.9 ns. After 5–10 ns there is no residual CL signal. When the device turns on the decay curve becomes more complex. The initial decay time, τ_i , increases to 5.3 ns at 2 V. However, there is a substantial residual CL signal which decays slowly with a decay time, τ_L , of about 700 ns. Since the buildup of this signal also has one fast and one slow component, the 50-ns e -beam pulse is not sufficiently long to reach steady state. This is demonstrated in Fig. 6 where the increase in CL during the e -beam pulse when the device is biased is clearly seen. For devices with

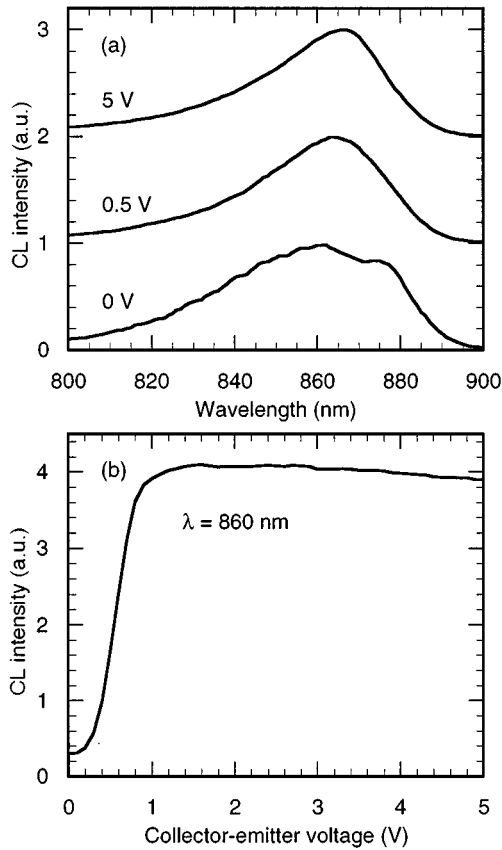


FIG. 4. CL intensity for a 6 QW device as function of (a) wavelength at different collector-emitter voltages and (b) collector-emitter voltage at 860 nm. Note that each spectrum has been normalized and has a baseline of 0, 1, and 2 units, respectively.

poor responsivity, where the CL intensity increases little or not at all when the voltage is increased, no such residual CL signal is observed indicating that the buildup in CL intensity seen in Fig. 4(b) is correlated to this slowly decaying CL signal and is a direct indicator of device performance. This can also be verified by changing the duty cycle of the e beam and studying the CL as a function of voltage. The increase in CL intensity is greatly affected by the duty cycle indicating that the process is slow.

To study the spectrum of this decay signal, CL-decay transients were taken at 0 and 1 V at each nm. Spectra from different time windows are shown in Fig. 7, where 0 ns is defined as the turnoff of the electron beam. The CL signal in each time window and wavelength is the integrated average over the time window indicated. At 0 V the peak at 860 nm has a very short decay time and after only 2 ns the peak at 880 nm dominates. After about 7 ns the residual CL signal is insignificant. At 1 V, however, the CL spectrum has a strong signal and the shape is intact even after 20 ns. No peak at 880 nm is seen. In both cases the main peak at 860 nm moves towards longer wavelengths with time.

Devices from the four different wafers were characterized. The only difference between the wafers was the number of absorbing QWs and thus the amount of lattice relaxation. The 6 QW structure has a total thickness of 480 Å absorbing material with both optical inspection and CL imaging show-

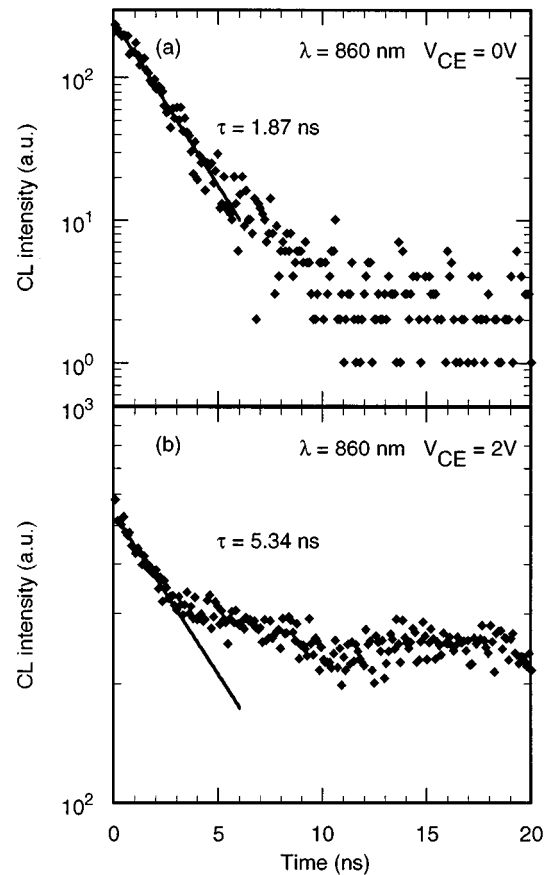


FIG. 5. CL-decay transients of a 6 QW device at 860 nm and collector-emitter voltages (a) 0 V and (b) 2 V. The lifetime, τ_i , increases from 1.87 to 5.34 ns as the device turns on.

ing that it is not relaxed. The 30 QW structure is heavily relaxed with extensive cross hatching on the surface. Both the CL and EBIC images (not shown here) showed much less contrast than expected.¹⁰ The difference between a ‘‘bright region’’ and a ‘‘dark region’’ was less than 3% in both the CL and the EBIC signals. Time resolved CL was

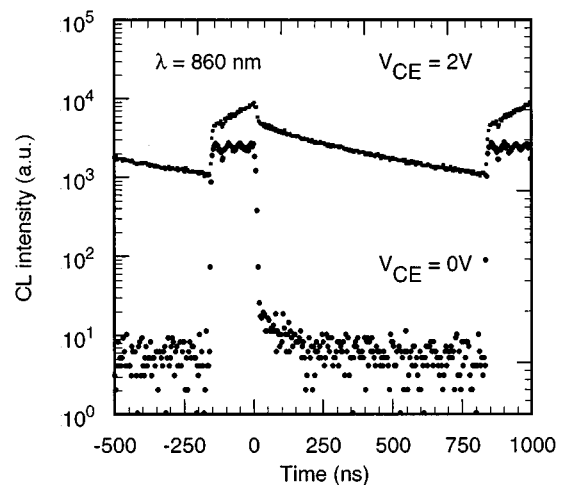


FIG. 6. Demonstration of slow CL buildup and decay when the device is turned on. The lifetime, τ_L , of this signal at 2 V is approximately 0.7 μ s.

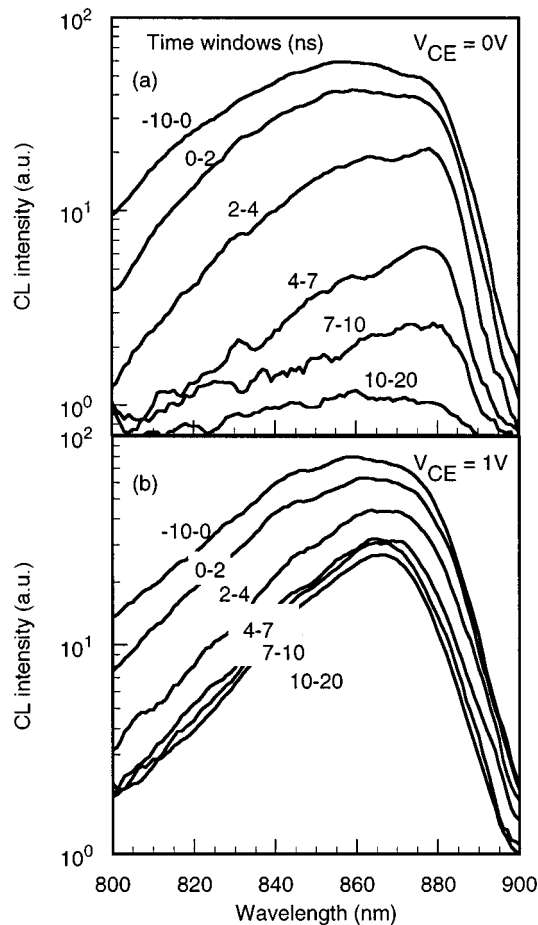


FIG. 7. Temporally resolved CL spectra at (a) 0 and (b) 1 V, respectively. The curves represent integrated averages over the time windows indicated.

performed on all structures. Figure 8 shows the initial decay time, τ_i , as a function of voltage for the four structures. There is no measurable difference between the 6 and 12 QW devices, both showing decay times, τ_i , of about 4 ns at 1 V collector-emitter voltage. For the other two structures, how-

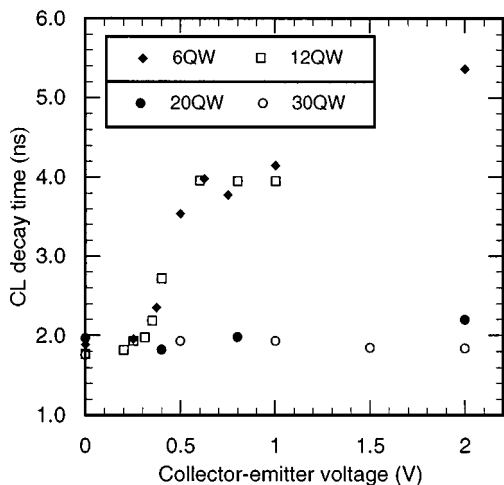


FIG. 8. CL decay time, τ_i , as a function of collector-emitter voltage for the 6, 12, 20, and 30 QW devices, respectively.

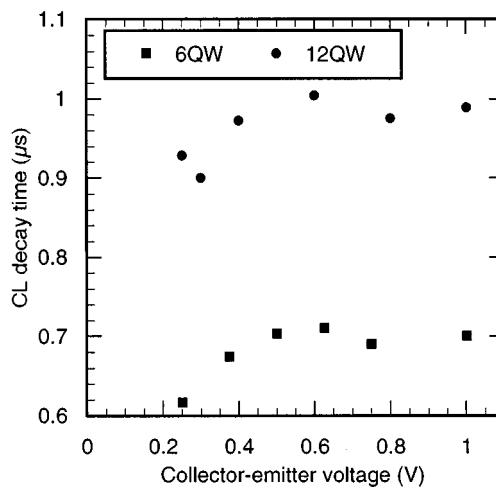


FIG. 9. CL decay time of the slowly decaying component, τ_L , as a function of collector-emitter voltage for the 6 and 12 QW devices.

ever, we see that the decay time decreases with relaxation indicating that relaxation will indeed reduce the carrier lifetime in the base. The 30 QW result is not representative since this device showed very poor responsivity and is therefore expected to have a much shorter lifetime. Devices with poor responsivity from the other three structures show similar decay times: 1.2 ns for the 6 QW, 1.8 ns for the 12 QW, and 1.6 ns for the 20 QW. In all these devices the decay time is independent of voltage. This suggests that the initial decay time, τ_i , is a good probe of device performance. The residual, slowly decaying CL, τ_L , shows a completely different relationship. As seen in Fig. 9, the decay time, τ_L , is 0.7 μ s for the 6 QW device and about 1 μ s for the 12 QW device. The decay time of the 20 QW device was too long to be measured with the current system setup, longer than approximately 2 μ s. There is no voltage dependence for this decay time.

We also studied the EBIC signal at different beam currents (and thus how the gain depends on the collector current) and were able to calculate the ideality factor of the devices. The ideality factor, n , of a device is a measure of the defect currents effect on the gain²⁴ and is defined by:

$$\beta \sim I_c^{(1-1/n)} \quad (1)$$

where β is the electrical gain and I_c is the collector current (or EBIC in our case). Figure 10 shows the EBIC as a function of beam current for the 6, 12, and 20 QW devices. The corresponding gain as a function of EBIC is shown in Fig. 11. Since there is a slight bending of these curves, the ideality factor for the devices are taken in two different EBIC regions, one below approximately 1 mA and one above. At low currents the 20 QW device has a much larger ideality factor, and less gain, than the 6 and 12 QW devices, at 2.3 compared to 1.7 and 1.8. At larger currents, however, the ideality factors are about the same for all three devices, at 1.4–1.7. In this large current region there is very little difference in gain between the devices indicating that some lattice relaxation is indeed tolerable without loss in performance if the current density is kept sufficiently high. By

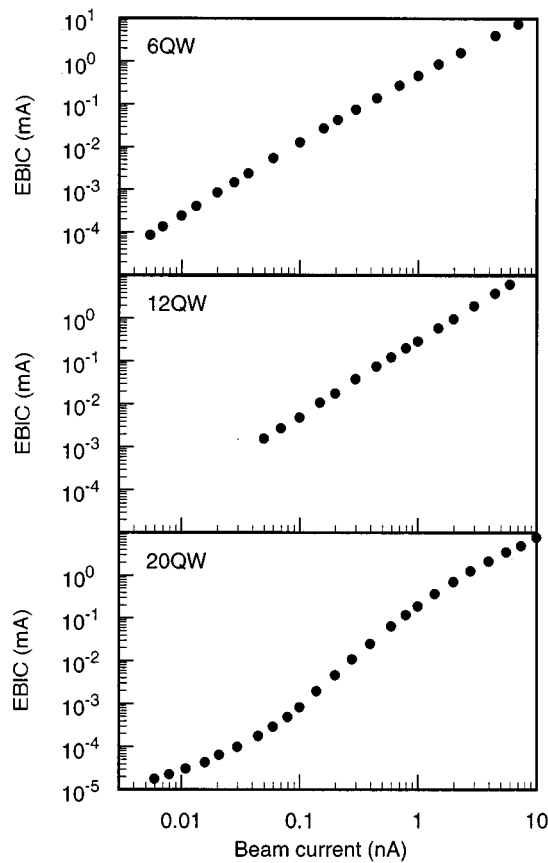


FIG. 10. EBIC as a function of beam current for devices with 6, 12, and 20 QWs.

studying the photocurrent as a function of beam current, the small signal ideality factor can be determined. For the 20 QW device we find that it has the same current dependence as the large signal ideality factor. The small signal ideality factor is 1.83 and 1.25, respectively, in the two current regions mentioned above.

A comparison between devices with good and poor responsivity, taken from the 20 QW wafer, shows that there are three distinct slopes, one with very low ideality factor, one with high ideality factor, and one with reasonable ideality factor. In the region with a low ideality factor the device has low gain and in the region with high ideality factor the gain is increasing rapidly. Normal HPT operation occurs in the third region. Whether a device is characterized as poor, with low gain and responsivity, or good, with high gain and responsivity, appears to be a matter of at which current density the measurement is performed, i.e., where the gain turns on. This is demonstrated in Fig. 12 where one device turns on at 100 nA EBIC and the other at 50 μ A. The ideality factor before turn on is 1.007 and there is no electrical gain in this region. After turn on the ideality factor is 2.3 for the good device and 7.4 for the poor device. At higher currents the slopes will again coincide and the ideality factor will be about 1.5 as mentioned above. Even the highly relaxed 30 QW low responsivity devices show this turn on but at slightly higher currents, about 70 μ A, and with ideality factors of 1.01 and 4.3, respectively.

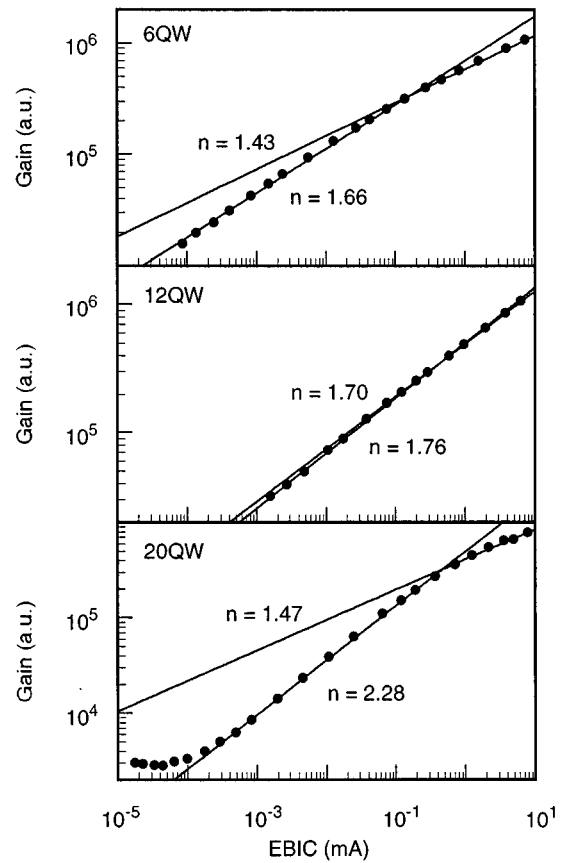


FIG. 11. From Fig. 10 corresponding gain as a function of EBIC. Estimated ideality factors in low current density and high current density regions are also shown.

IV. DISCUSSION

It is important to point out that the CL and EBIC versus collector-emitter voltage curves look exactly like the current-voltage plot for the transistor. By varying the beam current a

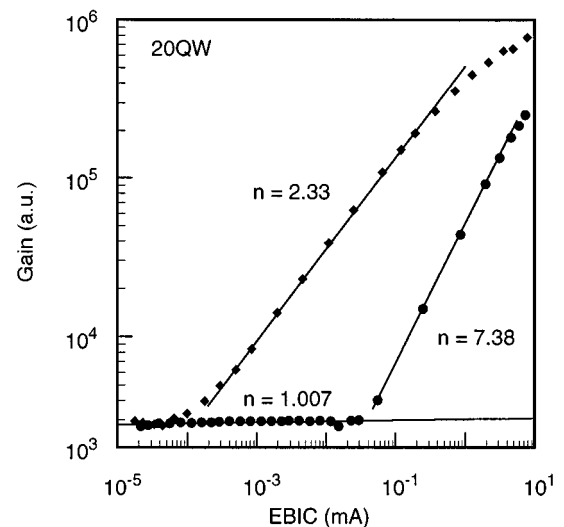


FIG. 12. Comparison of gain and ideality factors between two 20 QW devices, one showing high gain (\blacklozenge) and one showing low gain (\bullet) at 5 nA beam current. At sufficiently high currents the device with low gain turns on and the gain increases sharply.

Gummel plot with EBIC can be constructed. When the transistor turns on the current flow can increase by several orders of magnitude and this affects the CL signal so that it increases with the current flowing through the device, giving it the same voltage dependence as the current. This means that a high gain device will have a larger increase in CL with bias than a low gain device. The CL measurements show that the buildup in intensity can be more than an order of magnitude compared to the intensity at no bias. This can clearly be used as a measure of the quality of the device. Note that even at these high CL intensities only a very small fraction of the electrons recombine. This observed correlation between CL intensity and electrical gain can be qualitatively explained by considering the loss mechanisms of carriers in the device. The electrical gain is largely determined by the lifetime of holes in the base. In high quality material the predominant loss mechanism for holes is a direct, radiative recombination with electrons in the base-emitter heterojunction. This would lead to a high electrical gain and thus a large CL intensity. If, on the other hand, nonradiative loss mechanisms are present, such as defects at the base-emitter interface or relaxation induced misfit dislocations, the electrical gain, and the CL intensity, will be reduced. This measurement technique can thus give an indication of the relative strength of radiative and nonradiative recombination in the device which is an indirect measure of the material quality.¹⁰ By combining these measurements with the CL or PL measurements prior to device fabrication reported earlier in the literature,¹⁻⁸ a complete characterization of devices using CL or PL can be made. Several authors have reported that the *H*-band luminescence disappears when the Al content in the AlGaAs/GaAs heterojunction is graded.^{1,4} Use of a graded AlGaAs base has been suggested to enhance the electron transport through the base⁷ since grading will introduce a field in the conduction band which will result in electron drift across the base. A design like that should reduce recombination in the base. While this method may have drawbacks because of problems with Ohmic base contacts on AlGaAs for HBTs, it should prove to be an excellent design strategy for HPTs where no base contact is needed.

Based on the data presented above and previous luminescence measurements on heterojunctions reported in the literature,^{1,2,5} we believe that the fast decay transient of the CL signal comes from direct recombination in the base and the residual slow decay CL signal from spatially indirect recombination at the AlGaAs/GaAs heterojunction. This also explains why the CL intensity increases with applied voltage. When a voltage is applied there will be a slight field across the emitter and base trapping electrons in the notch at the conduction band discontinuity and the holes drift toward the valence band discontinuity in the base. Under bias, the energy difference between the AlGaAs conduction band and the notch is decreased and the probability of carriers tunneling out of the notch will be decreased. The presence of holes in the base will further accentuate this. The time resolved CL spectra show that the peak wavelength changes towards shorter wavelengths with time and that initially the 850 nm peak is dominant at both 0 and 1-V. The fact that the CL decays extremely fast at 0-V and very slowly at 1-V can be

explained in two ways. Either we see luminescence from two different regions but with approximately the same wavelengths or the redistribution of carriers in the absence of bias inhibits this indirect recombination very quickly after the excitation is turned off.

From the gain as a function of EBIC presented in Fig. 11 we see that at little or no lattice relaxation this follows the expected straight line. When relaxation is allowed, defects are normally formed at the GaAs/MQW/GaAs interface but some defects propagate through to the surface.¹⁰ The EBIC measurements indicate that in lattice relaxed material a certain current density is required for the ideality factor to be similar to that of nonrelaxed devices. This is most likely due to lattice defects filling up or whose local depletion regions decrease in size as the carrier concentration increases. At low current densities there is a high degree of nonradiative trap related recombination and at higher current densities these traps become filled and the associated nonradiative recombination is quenched leading to high electrical gain and a buildup in CL intensity. This means that relaxation is indeed tolerable and can lead to devices operating as well as nonrelaxed devices as long as the current, and thus the carrier concentration, is high enough.

The more relaxed devices show shorter decay times than the less relaxed devices. This indicates that the electrical gain for these devices is lower. However, previous measurement on these devices show that the 12 and 20 QW devices have similar electrical gain.³² Furthermore, these measurements showed the devices to have similar ideality factors. This does not mean that the CL decay time is a poor measure of the electrical gain. This difference can be explained by the fact that those measurements were taken at sufficiently high current.

V. CONCLUSIONS

We have performed time-resolved CL and EBIC measurements on partially relaxed AlGaAs/GaAs/InGaAs HPTs under operating conditions. The results show that the CL intensity increases more than an order of magnitude when the device turns on. Some devices had very low responsivity and these devices showed no such buildup in CL intensity indicating that this CL increase is correlated to the electrical gain of the device. Time resolved CL shows that the buildup in CL intensity is due to a very slow process that can be explained by spatially indirect recombination of electrons trapped in the notch formed at the conduction band discontinuity and holes in the base. Comparison between devices with a different amount of lattice relaxation indicates that relaxation is tolerable without catastrophic performance degradation. Relaxed samples have a more complex gain-current relationship with three distinct ideality factors. The current has to be sufficiently high to quench recombination related to strain induced lattice defects. At high currents a relaxed device operates as well as a nonrelaxed device.

ACKNOWLEDGMENTS

This work was financially supported by the Swedish Research Council for Engineering Sciences (TFR), the Swedish National Board for Industrial and Technical Development (NUTEK), ARO, and NSF (RIA-ECS).

- ¹Y. R. Yuan, K. Mohammed, M. A. A. Pudensi, and J. L. Mertz, *Appl. Phys. Lett.* **45**, 739 (1984).
- ²J. L. Bradshaw, W. J. Choyke, R. P. Devaty, and R. L. Messham, *J. Lumin.* **47**, 249 (1991).
- ³K.-S. Kim, J. B. Lee, B.-D. Choe, W. G. Jeong, and H. Lim, *Appl. Phys. Lett.* **65**, 451 (1994).
- ⁴K. Watanabe and K. Wada, *J. Cryst. Growth* **103**, 330 (1990).
- ⁵K. Eda and M. Inanda, *J. Appl. Phys.* **62**, 4236 (1987).
- ⁶C. Dubon-Chevallier, A. C. Papadopoulo, J. F. Bresse, and A. M. Duchenios, *J. Appl. Phys.* **66**, 2603 (1989).
- ⁷T. Humer-Hager and A. Asenov, *J. Appl. Phys.* **69**, 1583 (1991).
- ⁸Z. H. Lu, A. Majerfeld, P. D. Wright, and L. W. Yang, *IEEE J. Sel. Top. Quantum Electron.* **1**, 1030 (1995).
- ⁹J. M. Gilpérez, J. L. Sánchez-Rojas, E. Muñoz, E. Calleja, J. P. R. David, G. Hill, and J. Castagné, *Appl. Phys. Lett.* **61**, 1225 (1992).
- ¹⁰H. T. Lin, D. H. Rich, O. Sjölund, M. Ghisoni, and A. Larsson, *J. Appl. Phys.* **79**, 8015 (1996).
- ¹¹H. T. Lin, D. H. Rich, O. Sjölund, M. Ghisoni, and A. Larsson, *Appl. Phys. Lett.* **69**, 1602 (1996).
- ¹²A. Zemel and M. Gallant, *J. Appl. Phys.* **78**, 1094 (1995).
- ¹³M. A. Herman, D. Bimberg, and J. Christen, *J. Appl. Phys.* **70**, R1 (1991).
- ¹⁴J. Christen, M. Grundmann, and D. Bimberg, *J. Vac. Sci. Technol. B* **9**, 2358 (1991).
- ¹⁵J. C. Campbell, in *Semiconductors and Semimetals*, edited by W. T. Tsang (Academic, Orlando, 1985), Vol. 22, Part D, p. 389.
- ¹⁶See the special issue, Issue 2, on smart pixels, *IEEE J. Quantum Electron.* **29** (1993).
- ¹⁷See the special issue, Issue 6, on optical interconnects, *IEEE J. Lightwave Technol.* **13** (1995).
- ¹⁸See the special issue, Issue 8, on optical computing, *Appl. Opt.* **35** (1996).
- ¹⁹See the special issue, Issue 9, on semiconductor lasers, *IEEE J. Quantum Electron.* **27** (1991).
- ²⁰M. Yamaguchi, T. Yamamoto, K.-I. Yukimatsu, S. Matsou, C. Amano, Y. Nakano, and T. Kurokawa, *Appl. Opt.* **33**, 1337 (1994).
- ²¹G. R. Olbright, R. P. Bryan, K. Lear, T. M. Brennan, G. Poirer, Y. H. Lee, and J. L. Jewell, *Electron. Lett.* **27**, 216 (1991).
- ²²J. Bengtsson, N. Eriksson, and A. Larsson, *Appl. Opt.* **35**, 801 (1996).
- ²³R. S. Geels, B. J. Thibeault, S. W. Corzine, J. W. Scott, and L. A. Coldren, *IEEE J. Quantum Electron.* **29**, 2977 (1993).
- ²⁴N. Chand, P. A. Houston, and P. N. Robson, *IEEE Trans. Electron Devices* **ED-32**, 622 (1985).
- ²⁵T. G. Andersson, Z. G. Chen, V. D. Kulakovskii, A. Uddin, and J. T. Vallin, *Appl. Phys. Lett.* **51**, 752 (1987).
- ²⁶M. S. Ünlü, K. Kishino, J.-I. Chyi, L. Arsenaull, J. Reed, S. Noor Mohammed, and H. Morkoç, *Appl. Phys. Lett.* **57**, 750 (1990).
- ²⁷O. Sjölund, M. Ghisoni, and A. Larsson, *IEEE J. Quantum. Electron.* **33** (1997).
- ²⁸G. Bender, E. C. Larkins, H. Schneider, J. D. Ralston, and P. Koidi, *Appl. Phys. Lett.* **63**, 2920 (1993).
- ²⁹M. Ghisoni, G. Parry, L. Hart, C. Roberts, A. Marinopoulou, and P. N. Stavrinou, *Electron. Lett.* **30**, 2067 (1994).
- ³⁰L. P. Ramberg, P. M. Enquist, Y.-K. Chen, F. E. Najjar, L. F. Eastman, E. A. Fitzgerald, and K. L. Kavanagh, *J. Appl. Phys.* **61**, 1234 (1987).
- ³¹O. Sjölund, M. Ghisoni, and A. Larsson, *Electron. Lett.* **31**, 1870 (1995).
- ³²M. Ghisoni, O. Sjölund, A. Larsson, and S. M. Wang, *Appl. Phys. Lett.* **69**, 1773 (1996).
- ³³T. E. Everhart and P. H. Hoff, *J. Appl. Phys.* **42**, 5837 (1971).